PERGAMON

International Journal of Heat and Mass Transfer 45 (2002) 3233–3243

International Journal of HEAT and MASS TRANSFER

www.elsevier.com/locate/ijhmt

# Temperatures and the condensate heat resistance in dropwise condensation of multicomponent mixtures with inert gases

F.L.A. Ganzevles, C.W.M. van der Geld *

*Faculty of Mechanical Engineering, Eindhoven University of Technology, P.O. Box 513, 5600 MB Eindhoven, The Netherlands*

Received 27 October 2000; received in revised form 6 July 2001

**Abstract**

The temperature variations occurring in dropwise condensation at condenser plates of a compact, polymer heat exchanger are studied using instantaneous infrared temperature field recordings. An averaging procedure in time and an assessment of extreme values is proposed and carried out. With the results, the heat resistance of the condensate is quantified. It is found that mixing and convection in the condensate, caused by coalescence and drainage of drops, reduces the condensate heat resistance by a factor 4 as compared with purely conductive heat transfer. This reduction is comparable, both in nature and in magnitude, to the effect of enhanced mixing due to turbulence in the liquid film of filmwise condensation. A second condensable species has been added to the gas mixture in order to study the contribution of Marangoni convection due to concentration gradients to the condensate heat transfer resistance. No contribution is found. © 2002 Elsevier Science Ltd. All rights reserved.

*Keywords:* Dropwise condensation; Infrared thermography; Compact heat exchanger; Marangoni convection; Heat resistance; Mixing

## 1. Introduction

It is well known that dropwise condensation corresponds to high heat transfer coefficients [1–5]. For this reason, polymer plate condensers are an efficient means to recover heat from moist exhaust gases. Since the contact angle is about 90°, parts of these plates are covered by condensate drops, whereas smaller parts appear to be dry [6]. The plate is cooled from the inside (20 °C typically) and the bulk gas temperature is relatively high (80 °C typically). As a consequence, spatial temperature variation is high, not only in the downstream direction of the gas, but already at the scale of largest drop diameter (1.65 mm typically for moist air). In addition, the presence of inert gases may cause the interface temperature to vary at the interface of a single drop. Moreover, all temperatures fluctuate in the course of time since large drops drain off the plate, coalescing with smaller drops on the way down, see Fig. 1.

In this paper, the temperatures occurring in dropwise condensation on flat plastic plates are studied. Infrared measurements with high spatial resolution and high temperature resolution are used as a basis for the definition of averages and extremes.

Using these definitions and the infrared measurements it will be examined to what extend transfer inside condensate drops is conductive. The effect of drainage and coalescence of drops on the heat transfer in the condensate will be quantified. In the presence of inert gases, temperature variations may occur at the surface of condensate drops as the partial water vapour pressure may vary along the interface. These temperature variations are related to variations in surface tension coefficient, and therefore may cause convection inside condensate drops, so-called Marangoni convection. In an earlier study [7], the authors showed that this Marangoni convection can be enhanced by the presence of a second condensable species in the gas mixture. In the

* Corresponding author. Tel.: +31-40-2472923; fax: +31-40-2475399.

*E-mail address:* c.w.m.v.d.geld@tue.nl (C.W.M. van der Geld).


PII: S0017-9310(02)00026-1

**Nomenclature**

| | |
|---|---|
| $c_p$ | heat capacity at constant pressure (J/kg K) |
| $\vec{g}$ | acceleration due to gravity (m/s$^2$) |
| $\Delta H_{vap}$ | enthalpy of evaporation (J/kg) |
| $\dot{m}$ | mass flow rate (kg/s) |
| $Q$ | heat flow rate (W) |
| $q$ | heat flux (W/m$^2$) |
| $r$ | radius (m) |
| $T$ | absolute temperature (K) |
| $t$ | time (s) |
| $x$ | coordinate in gas flow direction (m) |
| $y$ | coordinate perpendicular to the gas flow direction (m) |

*Greek symbols*

| | |
|---|---|
| $\lambda$ | thermal conductivity (W/m K) |
| $\sigma$ | surface tension (N/m) |
| $\varphi$ | relative humidity (dimensionless) |
| $\omega$ | mass fraction (kg/(kg mixture)) |

*Indices*

| | |
|---|---|
| cond | condensate |
| cool | coolant |
| drop | droplet |
| eth | ethanol, $C_2H_5OH$ |
| g | gas |
| in | inlet |
| liq | liquid |
| max | maximum |
| min | minimum |
| out | outlet |

present study, air–steam–ethanol mixtures, with various concentrations of steam and ethanol, are therefore measured and analyzed. If the concentration gradients play a role of importance, different concentrations of ethanol in the gas mixture would yield different condensate heat resistances.

## 2. Experimental

### 2.1. Test rig

The wind tunnel, test section and main metering equipment was already described in earlier papers [3,6]. Main features, and a description of the new ethanol injection system, are given below.

Ambient air is blown in the wind tunnel (see Fig. 2) by two electrical fans (0.88 kW each), while 40 m downstream of the heat exchanger an extra fan is mounted. The maximum capacity is 2 m$^3$/s and can be controlled automatically or manually. Two heat exchangers (40 and 80 kW), supplied with steam at 7.8 bar, heat the air and a steam nozzle moistens the air with dry steam. The gas mixture passes the orifice with an inner diameter of 150 mm mounted according to DIN 1952 [8] in the tube with a diameter of 200 mm. The pressure drop over this orifice is measured with an inclined manometer, Airflow Developments LTD Lancaster RD England type

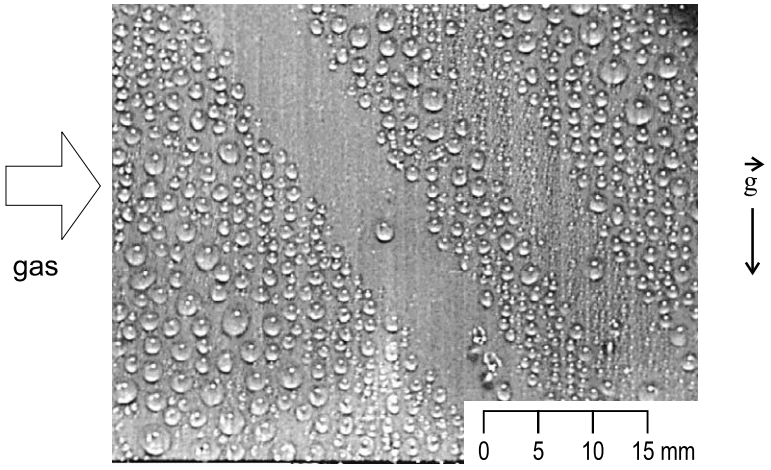


Fig. 1. Typical pattern during dropwise condensation due to drainage. Gas flows from left to right.

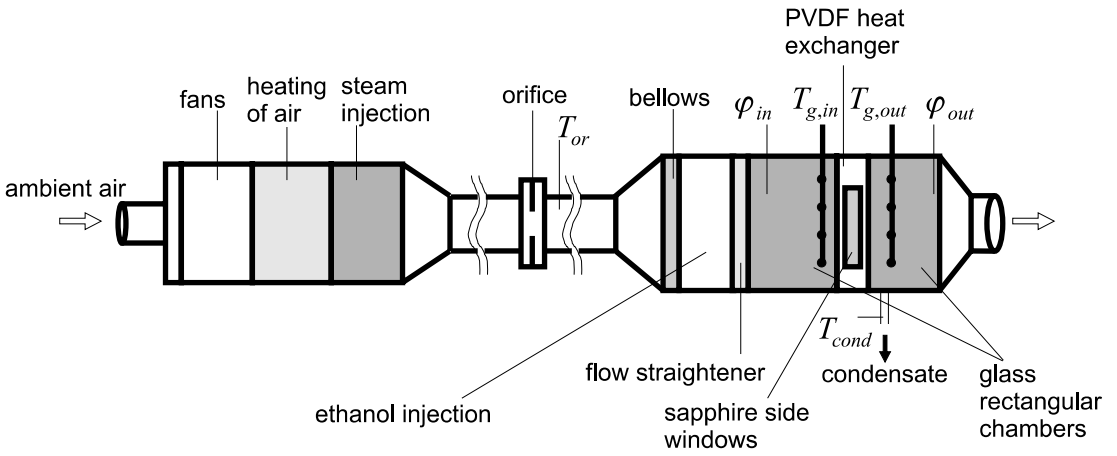


Fig. 2. Schematic of test rig. Only one of the measuring compartments is shown.

Mk 4 & 5, with an accuracy of 0.1% of full scale (1000 Pa). From this pressure drop, and the temperature, the mass flow rate is determined. The inlet gas mass flow rate, $\dot{m}_g$, is determined with accuracy better than 1%.

The gas mixture is split in two identical compartments, denoted as compartments I and II. In compartment II an injection system is mounted to make it possible to add ethanol to the gas mixture, see Fig. 2. Up- and downstream of the test heat exchanger, gas temperatures, $T_{g,in}$ and $T_{g,out}$, and relative humidities, $\varphi_{in}$ and $\varphi_{out}$, are measured. The temperatures are measured with thermoresistors, type Pt100 class A according to DIN IEC 751. Each sensor is made up from four of these thermoresistors. The relative humidity is measured with Vaisala HMP 135Y sensors with an accuracy of 1%. The sensors are calibrated using reference supersaturated salt solutions, lithium chloride and sodium chloride. At the outlet of the test unit a PolyvinyliTetraFluoride (PVTF) head has been mounted to prevent condensation inside the cap.

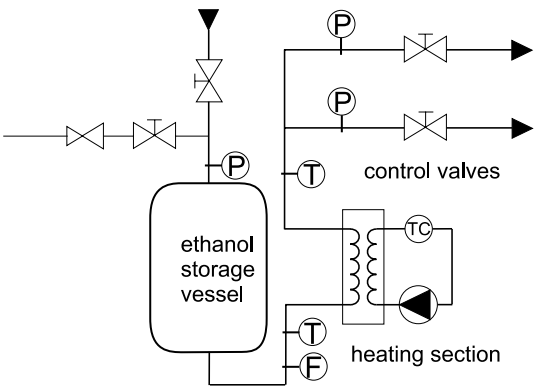


Fig. 3. Schematic of injection system.

In compartment II an injection system is mounted, see Fig. 3, to add ethanol to the gas mixture. The ethanol flow is measured with Fisher and Porter tri flat tube type No. FP-1/8-25-G-5/81 with a stainless steel float (bullet). The accuracy is within 0.1% of full scale ($6.60 \times 10^{-3}$ m$^3$/h). The liquid is atomised two meters upstream the test unit using one or two atomisers, type TX.60 Spraying Systems. The Sauter mean diameter is 44 μm measured with a Malvern Mastersizer at room temperature. The ethanol is evaporated within 0.7 m in co-current flow direction.

The coolant is water and the temperatures, $T_{cool,in}$ and $T_{cool,out}$, are measured for each compartment at the in- and outlet of the heat exchanger with a Pt100, accuracy 0.1 °C. The coolant mass flow rate, $\dot{m}_{cool}$, is measured with flow meters, type Fischer and Porter FP-1-35 G 10/80 stainless steel float 1-GNSVT-66, for each compartment individually with an accuracy better than 1% of full scale (0.77 kg/s).

The condensate is collected in catchers downstream the heat exchanger. In each collector a tube is mounted with a valve which leads the condensate to an Erlenmeyer flask. Upstream the valve, a Pt100 is mounted which measures the condensate temperature with an accuracy of 0.1 °C. The elapsed time and the weight of the condensate is measured to calculate the condensate mass flow rate.

The entire test rig is heated during more than five quarters of an hour prior to the actual measurements. The remaining inlet coolant temperature variation is less than 0.05 °C, as controlled by a PI device. The heat losses to the surroundings have been measured directly with two heat flux sensors, inaccuracy 1 W/m$^2$, with fluctuations due to draft etc. being 5 W/m$^2$ typically.

Typical histories of coolant and gas temperatures were presented in earlier papers, see e.g. [3], and exhibit the steadiness and reproducibility.

The test unit comprises 96 parallel, vertical PolyvinyliDeenFluoride (PVDF) plates. Each plate has 42 nearly rectangular coolant channels of $1.37 \times 1.47$ mm$^2$ and the distance between the centres of neighbouring coolant channels is 1.87 mm. The gas-sided wall thickness is 0.265 mm. The width of each plate is 2.00 mm. Each plate measures 400 mm in height and 76.3 mm in width. The distance in between two neighbouring plates is 2.0 mm. This gap is fixed by two reinforcements. Gas flows horizontally, in cross flow with the vertical coolant flow. Each compartment is separately measured and comprises 48 coolant plates.

### 2.2. Infrared camera and other optics

The wetted area ratio and the temperature field at two condenser sides are measured through two sapphire windows. Temperatures are measured contactless with an infrared (IR) camera, model thermovision system 680 (AGA infrared systems). The temperature range is adjustable and the temperature offset is arbitrary. The accuracy of temperature *differences* depends on the temperature range, which is in our case better than 0.04 °C. Absolute temperatures are obtained by comparing the intensity value during condensation with the intensity value of a reference black body object.

The attenuation depth of infrared light in the wave length range used, 2–5.6 μm, is for water negligible (0.1 mm) in comparison with the droplet size. In this wavelength window, absorption and emission of light in water are high, and reflection and transmittance are very low, so actually the condensate temperature at the gas–liquid interface is measured [9,10]. Similarly, if the condenser plate is dry the gas-sided plate temperature is measured. Due to condensate drainage, each location on each condenser plate is repeatedly swept dry. The absorption of light in the water vapor in the gas mixture is negligible because of the low concentration of water vapor (less than 20 wt%), and because the gas-layer thickness through which observations are performed is only 2 mm.

The following three types of calibration experiments were performed to check the outcomes of the IR-camera. In one experiment, the temperature of a cooled plate was first measured with a contact thermometer, and then a drop with a known, higher temperature was put on the plate. The temperature histories measured with the IR-camera were found to correspond properly to the surface temperature of the plate and the liquid–air temperature at the surface of the drop. These measurements are reported in [7]. Also, a hot plate at 400 °C was blocked with a thin water film at 20 °C. Again, the temperatures measured with the IR-camera showed that the gas–liquid interface temperature of the water was measured. In another experiment, an array of intrusive thermocouples was used to measure the temperature field in a water vessel that was locally heated from above. The IR-camera measured the horizontal water–air surface via a gold mirror from above. Again, the thermocouple readings were consistent with the IR-recordings. These measurements are reported in [10,11]. There is no doubt that the IR-camera is measuring the plate-surface and condensate-air interface temperatures that we aim to measure.

The signal from the cooled detector, InSb in liquid nitrogen, is digitised and stored on hard disk at a rate of 0.16 frames/s. Each image, $120 \times 128$ points, has an actual dimension of $50 \times 50$ mm$^2$, which is 610 pixels/cm$^2$. This gives each point a width of 0.4 mm. Frames are collected at a rate of 0.16 frames/s. Each infrared recording lasted for 500 s (8.3 min). The area of observation has been a circle with diameter 66 mm centred at the centre of the side of the condenser plate at the side of compartment II. Each IR-pixel measured $0.4 \times 0.4$ mm$^2$. The temperature *difference* accuracy depends on the bandwidth, but is typically $\pm 0.02$ K (0.04 K) for a bandwidth of 5 K (10 K).

A Hi8 video camera, Canon UC 2, and a photograph camera, Nikon F70 with an AF Micro Nikkor 60 mm macro objective and an Soligor Extension Tube 25, are used to measure the condensate drops via the sapphire inspection windows. The resolution of the photographic equipment is in this configuration 2 μm. Cool light illuminates the condenser surface and has no thermal influence at the condensate drops. The Hi8 video camera recordings, 25 frames/s, are used to obtain information of drainage since the drainage rate is typically 1 Hz in the area of observation. A digital high-speed camera, Kodak Ektapro HS Motion Analyzer, model 4540, $512 \times 512$ bits, operated at 500 Hz, is further used to investigate coalescence of drops.

### 2.3. Test matrix

A total of 24 process conditions have been studied using also infrared recordings. The following three categories of process conditions have been measured:

- Nine tests with condensation of air–steam mixtures. See Table 1 for process conditions.
- Eight tests with condensation of air–steam–ethanol mixtures with 0.0027 kg/(kg mixture) ethanol ($C_2H_5OH$). Other process conditions has been chosen essentially the same as with airsteam only, see Table 2.
- Seven tests with condensation of air–steam–ethanol mixtures with 0.0055 kg/(kg mixture) ethanol. Again essentially the same other process conditions as above have been employed, see Table 3.

Table 1
Process parameters for test with air–steam mixtures

| RUN | $T_{g,in}$ (°C) | $\dot{m}_{g,in}$ (kg/s) | $\omega_{vap,in}$ (kg/kg mixture) | $T_{cool,in}$ (°C) |
|---|---|---|---|---|
| E37230 | $73.3 \pm 0.1$ | 0.193 | 0.067 | $25.0 \pm 0.1$ |
| E57230 | $72.6 \pm 0.1$ | 0.216 | 0.067 | $24.94 \pm 0.07$ |
| E37148 | $71.8 \pm 0.1$ | 0.200 | 0.109 | $24.90 \pm 0.07$ |
| E57248 | $72.9 \pm 0.2$ | 0.216 | 0.109 | $24.90 \pm 0.07$ |
| E57065 | $71.0 \pm 0.2$ | 0.222 | 0.147 | $24.92 \pm 0.03$ |
| E58022 | $80.8 \pm 0.1$ | 0.216 | 0.077 | $24.88 \pm 0.06$ |
| E38038 | $81.1 \pm 0.2$ | 0.197 | 0.130 | $24.94 \pm 0.03$ |
| E58041 | $80.8 \pm 0.1$ | 0.214 | 0.143 | $24.98 \pm 0.05$ |
| E58062 | $80.5 \pm 0.4$ | 0.220 | 0.228 | $24.94 \pm 0.03$ |

For $T_{cool,in}$ the standard deviation (95% reliability) of 100 data is given. The measured errors of $T_{cool,in}$ and $T_{g,in}$ are 0.1 °C, see Section 2.1.

Table 2
Inlet process parameters for tests with air–steam–ethanol mixtures with 0.0027 kg/(kg mixture) ethanol

| RUN | $T_{g,in}$ (°C) | $\dot{m}_{g,in}$ (kg/s) | $\omega_{vap,in}$ (kg/kg mixture) | $\omega_{eth}$ (kg/kg mixture) | $T_{cool,in}$ (°C) |
|---|---|---|---|---|---|
| E37230 | $74.6 \pm 0.2$ | 0.195 | 0.064 | 0.0027 | $24.91 \pm 0.08$ |
| E57230 | $72.1 \pm 0.2$ | 0.216 | 0.067 | 0.0024 | $24.93 \pm 0.07$ |
| E37148 | $71.5 \pm 0.2$ | 0.200 | 0.108 | 0.0027 | $24.95 \pm 0.03$ |
| E57248 | $72.9 \pm 0.2$ | 0.215 | 0.110 | 0.0025 | $24.9 \pm 0.1$ |
| E58022 | $79.7 \pm 0.2$ | 0.216 | 0.078 | 0.0025 | $24.88 \pm 0.05$ |
| E38038 | $80.5 \pm 0.2$ | 0.198 | 0.129 | 0.0027 | $24.91 \pm 0.03$ |
| E58041 | $79.9 \pm 0.2$ | 0.213 | 0.142 | 0.0025 | $24.94 \pm 0.01$ |
| E58062 | $78.8 \pm 0.1$ | 0.219 | 0.228 | 0.0025 | $24.89 \pm 0.04$ |

Table 3
Inlet process parameters for tests with air–steam–ethanol mixtures with 0.0055 kg/(kg mixture) ethanol

| RUN | $T_{g,in}$ (°C) | $\dot{m}_{g,in}$ (kg/s) | $\omega_{vap,in}$ (kg/kg mixture) | $\omega_{eth}$ (kg/kg mixture) | $T_{cool,in}$ (°C) |
|---|---|---|---|---|---|
| E37230 | $72.8 \pm 0.2$ | 0.192 | 0.064 | 0.0055 | $25.03 \pm 0.05$ |
| E57230 | $72.7 \pm 0.3$ | 0.213 | 0.065 | 0.0050 | $24.96 \pm 0.06$ |
| E37148 | $74.2 \pm 0.3$ | 0.198 | 0.110 | 0.0054 | $24.95 \pm 0.03$ |
| E57248 | $71.8 \pm 0.2$ | 0.215 | 0.109 | 0.0050 | $24.90 \pm 0.06$ |
| E38038 | $82.1 \pm 0.1$ | 0.197 | 0.127 | 0.0055 | $24.92 \pm 0.02$ |
| E58041 | $81.1 \pm 0.4$ | 0.213 | 0.137 | 0.0051 | $24.89 \pm 0.03$ |
| E58062 | $81.9 \pm 0.3$ | 0.219 | 0.220 | 0.0050 | $24.93 \pm 0.05$ |

## 3. Measured interface and plate temperature profile histories

Figs. 4 and 5 show typical interface temperature history plots during condensation of air–steam and air–steam–ethanol mixtures, respectively. Fig. 6 is an enlargement of a single droplet of Fig. 4. It shows that temperature gradients occur at the drop interface. After 5 s the drop is seen to move away. The temperature at the top of a drop decreases in gas flow direction, see Fig. 7. This temperature increases with increasing droplet diameter, see Figs. 4, 5 and 7.

## 4. Temperature extremes and interpretation

Coordinates in flow direction, $x$, and along the vertical, $y$, are employed (see Fig. 5). The variation of temperature in $y$-direction is in Fig. 4 seen to be caused mainly by the local condensate height. Let $T_{y\max}$ be defined by

$$T_{y\max}(x,t) \equiv \max_i T(x,y_i,t), \tag{1}$$

where $i \in [1,85]$ numbers the pixels of an instantaneous IR-recording for a constant $x$-value (see Fig. 8).

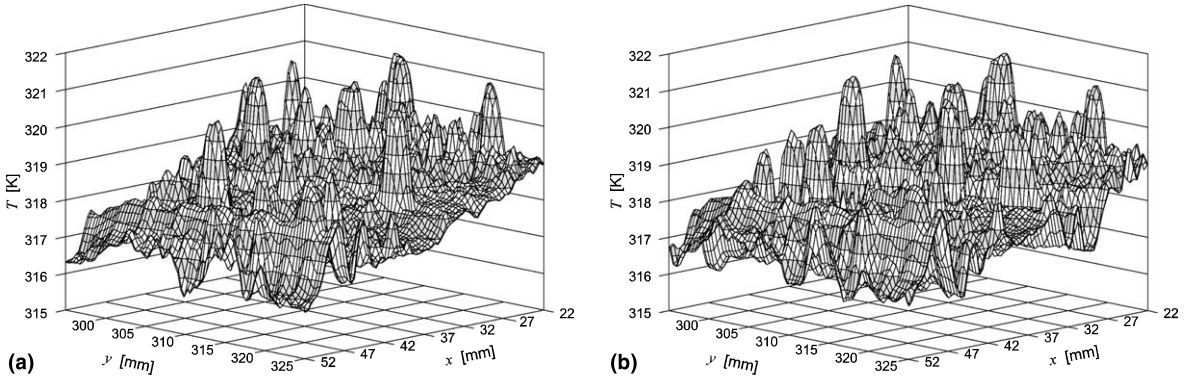


Fig. 4. History of temperature field on a condenser plate at $t = t_0$ and $t = t_0 + 5$ s. Area shown measures $80 \times 80$ pixels and each pixel measures $0.38 \times 0.38$ mm$^2$. Temperature resolution is 0.04 K during measurement; each grey intensity corresponds to a bandwidth of 0.5 K. Condensation of air–steam on a vertical, PVDF plate. For process conditions see Table 1 run E38038.

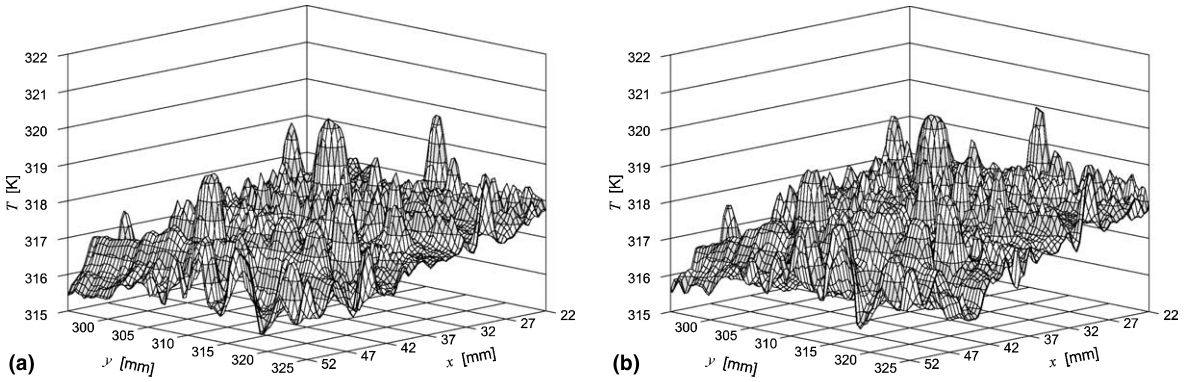


Fig. 5. History of temperature field on a condenser plate with condensation of air–steam–ethanol at $t = t_0$ and $t = t_0 + 5$ s, with ethanol concentration of 0.55 wt% in air. For process parameters see run E38038 in Table 3.

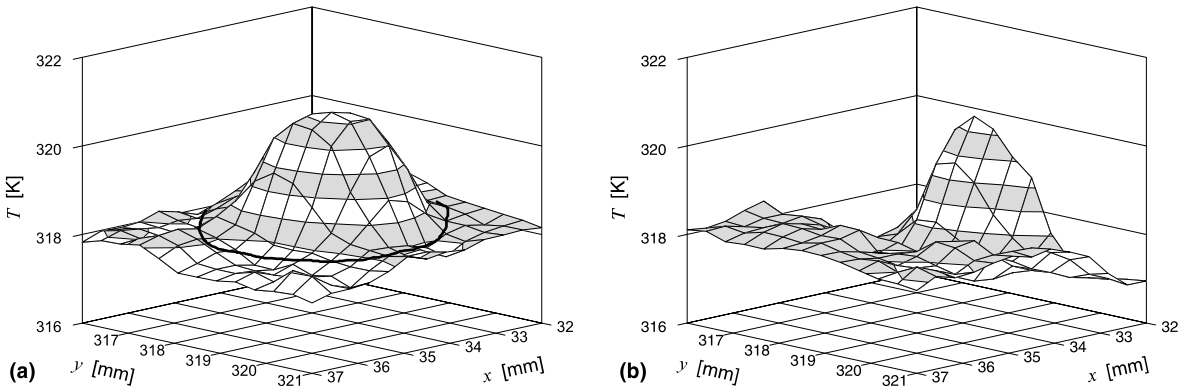


Fig. 6. Interfacial temperature field of a typical drop during condensation of water vapour at: (a) $t = t_0$; (b) $t = t_0 + 5$ s. For process parameters see run E38038 in Table 1.

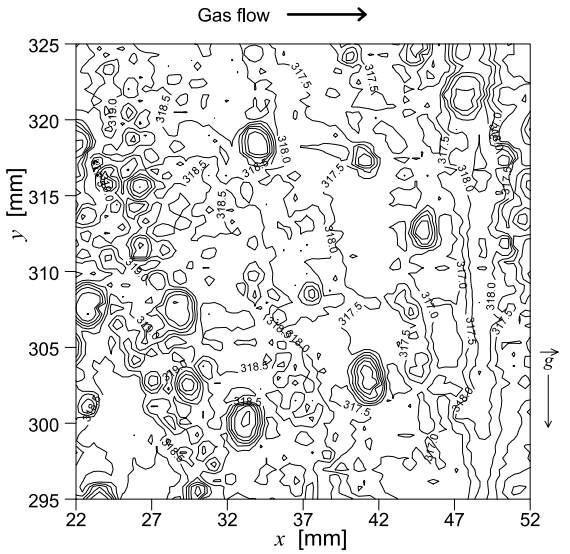


Fig. 7. Isotherms of actual condensation of an air–steam mixture, see for process parameters run E38038 in Table 1. The gas mixture flows from left to right.

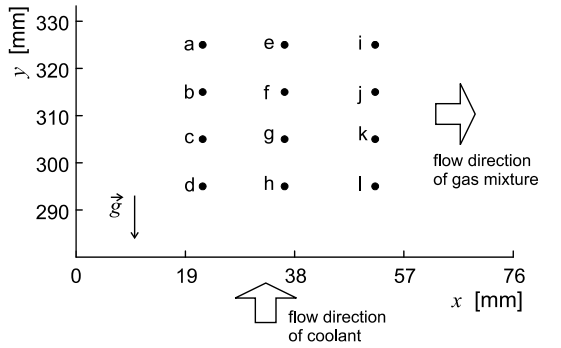


Fig. 8. Definition of coordinate system and locations a–l.

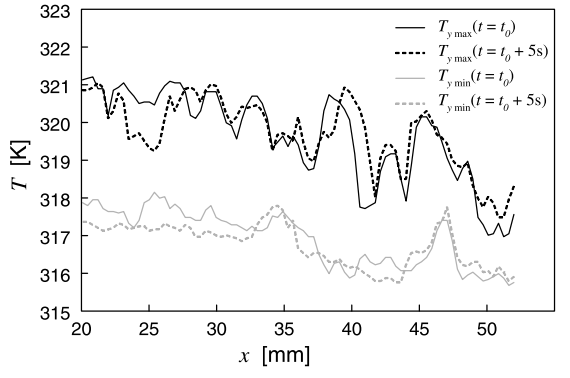


Fig. 9. Typical histories of $T_{y\max}$ and $T_{y\min}$ at various positions in gas flow direction, $x$, For process parameters of run E38038 in Table 1.

Temperature $T_{y\min}$ is defined similarly. Note that each pixel gives a temperature averaged over $0.4 \times 0.4$ mm$^2$. Temperature $T_{y\max}$ therefore might be a little less than the actual maximum occurring at fixed $x$-position. The coolant temperature varies by 0.5 K maximum in the area of observation. The difference in $T_{y\max}$ and $T_{y\min}$ at arbitrary $x$-position, see Fig. 9, is mainly due to differences in height of the condensate drops on the surface. If at time $t_0$ a large drainage drop passes $x_0$, $T_{y\max}(x_0,t_0)$ is increased, while immediately thereafter $T_{y\min}(x_0)$ is lowered because of the dry track that is left behind at $x_0$ by the drainage drop. If at position $x_0$ the maximum temperature, corresponding to the largest drop, is to be determined, for reasons to be explained in Section 5, we therefore have to take the maximum value in the course of time, i.e.

$$\langle T_{y\max}\rangle_{t\max}(x) \equiv \max_j\left\{\max_i T(x,y_i,t_j)\right\},$$

where $j \in [1,100]$ numbers the times at which IR-recordings are taken. The interpretation of the results of the averaging in time is complicated by the number of timescales that are involved:

- the rapid initiation of nuclei,
- the growth of drops by diffusion,
- the time between subsequent drop confluences,
- the drainage rate by large drops migrating downward.

To cover all phenomena, the observation time has to be an order of magnitude larger than the largest timescale involved, which is the last one listed above. The time between subsequent sliding off of large drops from $50 \times 50$ mm$^2$ of plate area depends on inlet gas temperature and inlet gas humidity mainly and is named drainage time. The drainage time, $t_{\mathrm{drain}}$, is typically 5 s for moist air conditions. The observation time has therefore been chosen to be 500 s. Note that the operators $\langle\rangle_{t\max}$ and $\langle\rangle_{y\max}$ commutate, as do $\langle\rangle_{t\min}$ and $\langle\rangle_{y\min}$ that are defined similarly. The use of time-averaging, e.g. with

$$\langle T\rangle_{t\,\mathrm{mean}}(x,y) \equiv \underset{j}{\mathrm{mean}}\{T(x,y,t_j)\} \tag{2}$$

is not recommended since, for example, in general

$$\left\langle\langle T\rangle_{t\,\mathrm{mean}}\right\rangle_{y\max}(x) \leqslant \left\langle\langle T\rangle_{y\max}\right\rangle_{t\,\mathrm{mean}}(x) \tag{3}$$

but usually the LHS of Eq. (3) turns out to be less than the RHS. This implies that the operators $\langle\rangle_{t\,\mathrm{mean}}$ and $\langle\rangle_{y\max}$ in common practise do not commutate.

Fig. 10 shows typical profiles of $\langle T_{y\max}\rangle_{t\max}(x)$ and $\langle T_{y\min}\rangle_{t\min}(x)$. At $x = 47$ mm a spatial raise in the minimum temperature $\langle T_{y\min}\rangle_{t\min}$ is found. This location corresponds to the place where a single coolant channel

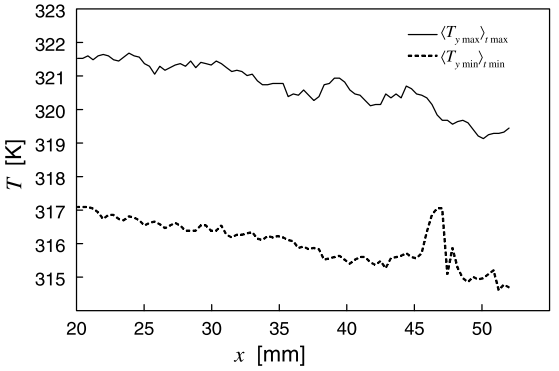


Fig. 10. Variation of maximum and minimum temperature in gas flow direction, $x$, For process parameters of run E38038 in Table 1.

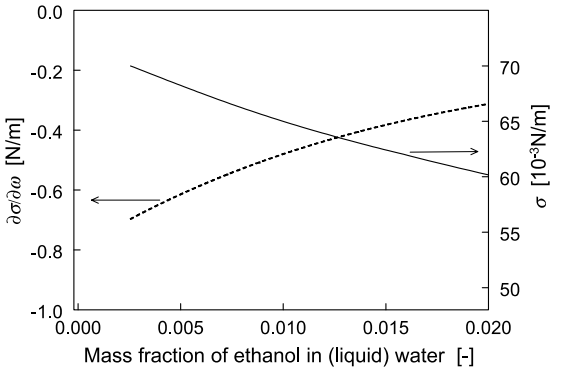


Fig. 11. Surface tension gradient and surface tension of water–ethanol mixtures at 298 K.

was blocked to investigate its effect on plate temperatures. It is obvious that the plate temperature should be higher at this place than at other places. The local raise of only $\langle T_{y\min}\rangle_{t\min}$, and not of $\langle T_{y\max}\rangle_{t\max}$, therefore supports the interpretation, that $\langle T_{y\min}\rangle_{t\min}$ is the local $(x)$ plate temperature and $\langle T_{y\max}\rangle_{t\max}$ the local maximum temperature of the largest drainage drops. As the example of Fig. 10 shows, this maximum temperature varies in flow direction.

Since $t_{\text{drain}}$ is about 5 s, most of the observed plate is covered by 'stationary' drops, see Fig. 1. These drops adopt to the local gas temperature and have the largest contribution to $\langle T_{y\max}\rangle_{t\max}$ and $\langle T_{y\min}\rangle_{t\min}$ (immediately after moving away). The large drainage drops follow trajectories at an angle with the vertical, see Fig. 1, and transport condensate from the upstream gas flow direction to places downstream. However, on their way down and downstream these large drainage drops coalesce with smaller drops that are adopted to the local gas temperature. Also, this mixing process is relatively slowly. As a result, $\langle T_{y\max}\rangle_{t\max}$ is hardly affected by drainage drops coming from high-temperature regions. More details about coalescence and drainage process are reported in another paper [12].

## 5. The condensate heat resistance

With the aid of the infrared measurements described above, the heat transfer inside condensate drops will now be investigated. In particular, this heat transfer will be quantified, and compared with purely conductive heat transfer in the condensate, in a way that if customary for film condensation [1]. Note that all our measurements are for dropwise condensation.

Differences between actual and purely conductive heat transfer are expected to be due to flow- and gravity-induced convection and mixing inside condensate drops, and maybe due to Marangoni convection inside drops. Marangoni convection is caused by surface tension gradients which can be due to temperature gradients and/or concentration gradients since condensation is from air–vapor mixtures with a large amount of non-condensibles, see Section 1. The contribution of Marangoni convection in the condensate drops to heat transfer will be varied in our experiments to single out the Marangoni effect due to concentration gradients, the so-called destillocapillary effect. To this end, air–steam–ethanol mixtures with varying concentration of ethanol are condensed in an actual heat exchanger, a compact polymer one. The Marangoni convection due to temperature gradients is promoted by the occurrence of a soluble component in the gas mixture, as single-drop experiments of an earlier study showed [7]. Any systematic trend in condensate heat transfer as a function of the concentration ethanol in the gas might indicate the occurrence of Marangoni convection. Experiments have been performed with three inlet mass fractions of ethanol: $\omega_{\text{eth,in}} = 0$, $\omega_{\text{eth,in}} = 0.0025$ and 0.0050 kg/(kg mixture), see Section 2. The values of $\omega_{\text{eth}}$ have been selected such, that the surface tension gradients $\partial\sigma/\partial\omega_{\text{eth}}$ are relatively large, see Fig. 11. Note that $\omega_{\text{eth,liq}}$ depends on $\omega_{\text{eth,vap}}$ and temperature. In equilibrium, $\omega_{\text{eth,vap}}$ is about twice $\omega_{\text{eth,liq}}$ at the same temperature. Direct measurement, with a densitometer, of $\omega_{\text{eth,liq}}$ in the condensate yielded values of about 0.01, indicating the condensate drop residence time is long enough to reach equilibrium. Fig. 11 shows $\sigma$ and $\partial\sigma/\partial\omega$ for values of $\omega_{\text{eth,liq}}$ around 0.01. In the following, measurements for the three inlet mass fractions of ethanol are discussed simultaneously.

Recordings like shown Figs. 9 and 10, for various concentrations of ethanol and water vapor in the gas mixture, suggest that the time-averaged temperature $\langle T\rangle_{t\,\text{mean}}$ is a smooth continuous function of coordinates $x$ and $y$. The maximum value of $\langle T\rangle_{t\,\text{mean}}$, $\langle T_{y\max}\rangle_{t\max}$, corresponds to the temperature at the top of large

condensate drops that are about to be draining off the condenser plate, see Section 4. The minimum value of $\langle T\rangle_{t\,\mathrm{mean}}$, $\langle T_{y\,\mathrm{min}}\rangle_{t\,\mathrm{min}}$, corresponds to the gas-sided temperature of the condenser plate, see Section 4. These time-averaged temperatures will be used in the following analysis of heat transfer in the condensate.

In an earlier paper [3], temperatures in a flowing gas mixture and in a drop on a flat plate were numerically computed. Heat transfer in the condensate was assumed to be purely conductive. The main conclusion drawn from these computations is that isotherms inside drops are nearly equidistant and parallel to the condenser plate. The principle reason for this is the uniform distribution of the heat liberated by condensation at the drop interface. As a result of the isotherms being parallel and equidistant, the conductive heat flux in the condensate is given by

$$q_{\mathrm{conductive}} = \lambda_{\mathrm{cond}} \cdot \left(\left\langle T_{y\,\mathrm{max}}\right\rangle_{t\,\mathrm{max}} - \left\langle T_{y\,\mathrm{min}}\right\rangle_{t\,\mathrm{min}}\right)/r_{\mathrm{drop,max}}.$$

Here $\lambda_{\mathrm{cond}}$ is the heat conductivity of the condensate (water). Values of parameters occurring in this expression of $q_{\mathrm{conductive}}$ will now be evaluated for the test conditions of Section 2.3.

The maximum drop radius, $r_{\mathrm{drop,max}}$, measured is 1.65 mm $\pm 10\%$ for air–steam and 1.5 mm $\pm$ 10% for air–steam–ethanol, for both nonzero values of $\omega_{\mathrm{eth,in}}$. The given error is twice the standard deviation [13]. The temperature difference $(\langle T_{y\,\mathrm{max}}\rangle_{t\,\mathrm{max}} - \langle T_{y\,\mathrm{min}}\rangle_{t\,\mathrm{min}})$ is nearly independent of coordinate $x$, see Fig. 10. Fig. 12 shows values of this temperature difference which have been obtained using the analysis of infrared recordings described in Section 4. Errors in this Fig. 12 are computed using RMS values and the method described by Kline and McClintock [13]. Below, resulting values for $q_{\mathrm{conductive}}$ will be compared with the actual heat flux through the condensate.

Most of the heat extracted from the gas mixture flows through condensate drops, as is shown by the following considerations. Let the percentage of convective heat transfer from the gas to the coolant be quantified by the parameter $F_{\mathrm{conv}}$, defined by

$$F_{\mathrm{conv}} = \frac{Q_{\mathrm{cool}} - \dot{m}_{\mathrm{cond}} \cdot \Delta H_{\mathrm{vap}}}{Q_{\mathrm{cool}}} \cdot 100\%$$

with $\Delta H_{\mathrm{vap}}$ the condensation enthalpy and $\dot{m}_{\mathrm{cond}}$ the measured condensate mass flow rate. Measured values of $F_{\mathrm{conv}}$ show [14,15] that for $\omega_{\mathrm{vap,in}} > 0.1$, i.e. for the moist air condition prevailing in our measurements, $F_{\mathrm{conv}}$ is less than 10%, meaning that convective heat transfer to drops *and* plate is less than 10% of the total heat transfer. Since heat transfer from the gas *not* through the condensate, i.e. directly to the condenser plate, can only be convective, most heat transfer from the gas is through the condensate drops.

A measure for the deviation of actual heat transfer from purely conductive heat transfer through the condensate is the parameter $F_{\mathrm{Maran}}$ defined by

$$F_{\mathrm{Maran}} \equiv q_{\mathrm{cool}}/q_{\mathrm{conductive}}. \tag{4}$$

Here $q_{\mathrm{cool}}$ is the heat flux to the coolant through the condensate. Since most of the heat transfer from the gas to the coolant goes via the condensate, as discussed above, the heat flux $q_{\mathrm{cool}}$ can be determined from the total heat flux to the coolant, i.e.

$$q_{\mathrm{cool}} = \dot{m}_{\mathrm{cool}} \cdot \left(c_{\mathrm{p,cool}}(T_{\mathrm{cool,out}}) \cdot T_{\mathrm{cool,out}} - c_{\mathrm{p,cool}}(T_{\mathrm{cool,in}}) \cdot T_{\mathrm{cool,in}}\right)/A_{\mathrm{comp}} \tag{5}$$

with $\dot{m}_{\mathrm{cool}}$ the coolant mass flow rate to one compartment and $A_{\mathrm{comp}}$ is the corresponding surface area. Values of $F_{\mathrm{Maran}}$ deduced from the measurement results are displayed in Fig. 13. The mean value of $F_{\mathrm{Maran}}$ is 4, with

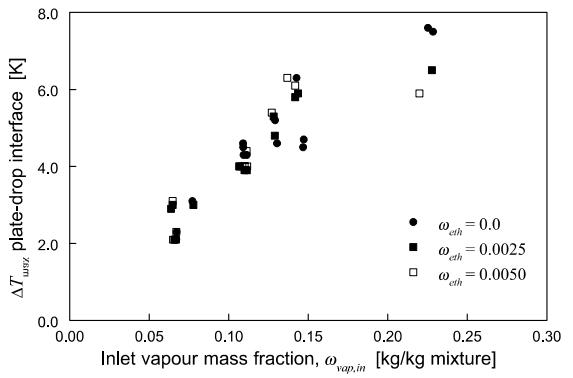


Fig. 12. Comparison of maximum temperature difference measured with infrared for drops of pure water and water–ethanol mixtures. The error is 0.5 K for $\omega_{\mathrm{vap,in}} > 0.1$ and 0.4 K for $\omega_{\mathrm{vap,in}} < 0.1$ the difference due to different ranges of the infrared camera.

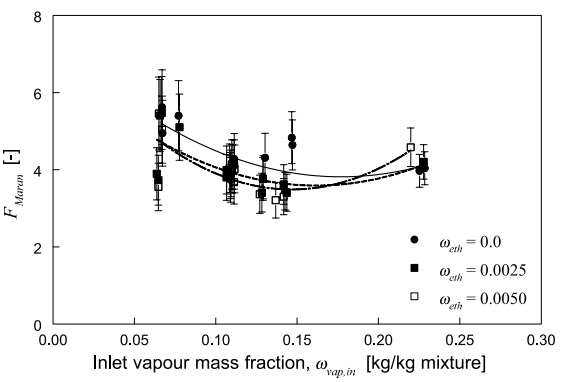


Fig. 13. Measurements of the ratio of measured heat flux to the coolant and to the estimated conductive heat flux due in drops, $F_{\mathrm{Maran}}$.

only a weak dependence on $\omega_{vap,in}$. The value of $F_{Maran}$ being significantly larger than 1 shows that conduction underestimates heat transfer in the condensate.

It is concluded that the mixing caused by coalescence and drainage, possibly in combination with an effect of thermocapillary convection, dominates heat transfer through the condensate. There is a continual refreshing of liquid that is in contact with the gas, as is confirmed by the temperature field histories measured with the infrared camera, see Figs 4, 5 and 9. In addition, temperature-driven Marangoni convection, the so-called thermocapillary effect, is bound to occur since temperature gradients are measured on the gas–liquid interface of individual condensate drops, see Fig. 6. The typical temperature drop measured, 2 °C, was in an earlier study [7] shown to create vortical motion near the contact line inside the condensate drop. Such motion obviously enhances heat transfer.

No systematic trend of $F_{Maran}$ as a function of $\omega_{eth}$ is observed in Fig. 13, since the destillocapillary effect is outweighed by the combination of enhanced mixing and thermocapillary convection.

In is interesting to compare the above effect of mixing on *dropwise* condensation with the effect that enhanced mixing, due to turbulence, has on heat transfer during *filmwise* condensation. Colburn [1] predicted the ratio of the actual mean heat transfer coefficient in a (partly) turbulent condensate film to that predicted for a purely laminarly flowing condensate film. For effective film Reynolds numbers, $Re_f$, exceeding 10 000 and for Prandtl numbers exceeding 1, this ratio was found to be 3 at minimum, and increasing with increasing Reynolds number and with increasing Prandtl number. Here $Re_f$ is the ratio $4\Gamma/\eta_f$ with $\eta_f$ the dynamic viscosity of the liquid film and $\Gamma$ the mass flow rate per unit width. The values of around 4 in Fig. 13 are fully comparable with the ratios found by Colburn. The physical mechanism of enhanced mixing has apparently the same effect in dropwise condensation as it has in filmwise condensation.

The following remarks are made regarding checks of these measurements using reference data and correlations.

Typical values of the net heat transfer coefficient, $h_{tot}$, from the gas to the plate are 150–200 $W/m^2$ K, see, for example, [16]. Due to the high concentration of non-condensibles in the gas mixtures of this study, and due to the condensation being dropwise rather than filmwise, no data obtained by other people have been found in the literature to compare our values of $h_{tot}$ with. It is, however, possible to validate the gas-sided plate temperatures found with the above analysis of infrared recordings, by comparison with inlet and outlet plate temperatures obtained in another way. This is reported in another paper [12]. In addition it is possible to validate the condensate-gas interface temperatures provided by our analysis, by calculating heat transfer coefficients and comparing them with those obtained with mock-up experiments described in an earlier paper [3]. For sake of conciseness and clarity this will be done in a subsequent paper [17].

## 6. Conclusions

In downstream direction of the gas, $x$, temperature variation is considerable (50 °C/m or more). At each $x$, the spatial and temporal extremes $\langle T_{y\max}\rangle_{t\max}$ and $\langle T_{y\min}\rangle_{t\min}$ are defined and determined using infrared recordings. The differences between these two extremes, $\Delta T$, is approximately independent of streamwise location, $x$.

With $q_{cool}$ the measured heat flux to the coolant, and with $q_{conductive}$ given by $\lambda_{cond}\cdot\Delta T/r_{drop,max}$, the parameter $F_{Maran}=q_{cool}/q_{conductive}$ is a measure of the heat resistance of the condensate. The mean measured value of $F_{Maran}$ is about 4, with only a weak dependence on the water vapour concentration, $\omega_{vap,in}$ in kg/(kg mixture). The mixing in the condensate and the continual refreshing of liquid in contact with the gas, by coalescence and drainage of condensate drops, possibly in combination with surface-tension driven convection inside drops, explain the value of $F_{Maran}$. This effect of enhanced mixing on heat transfer for *dropwise* condensation is much similar to the effect of enhanced mixing, due to turbulence, on heat transfer for *filmwise* condensation. In similar process conditions, this effect has even the same magnitude for dropwise condensation as it has for filmwise condensation.

No effect of the concentration of ethanol in the gas mixture, $\omega_{eth}$, is found, so concentration gradients add little to the convection and mixing in the condensate.

## References

[1] J.G. Collier, J.R. Thome, in: Convective Boiling and Condensation, Clarendon Press, Oxford, 1994, p. 450 (Chapter 10).
[2] A. von Eucken, Energie- und Stoffaustausch an Grenzflächen, Die Naturwissenschaften 25 (1937) 209–218 (in German).
[3] F.L.A. Ganzevles, C.W.M. van der Geld, Heat and mass transfer from internal flows to hemispheres and flat parts in between, Int. J. Heat Mass Transfer 41 (1998) 3705–3718.
[4] D.W. Tanner, C.J. Potter, D. Pope, D. West, Heat transfer in dropwise condensation – Part I, The effects of heat flux, steam velocity and non condensable gas concentration, Int. J. Heat Mass Transfer 8 (1965) 419–426.
[5] D.W. Tanner, D. Pope, C.J. Potter, D. West, Heat transfer in dropwise condensation at low steam pressures in the absence and presence of non-condensable gas, Int. J. Heat Mass Transfer 11 (1968) 181–190.

[6] F.L.A. Ganzevles, C.W.M. van der Geld, In-situ measurements of wetting rate and local temperatures with dropwise condensation in a compact heat exchanger, in: Proceedings of the 30th National Heat Conference, HTD-314, vol. 12, ASME, New York, 1995, pp. 68–76.
[7] F.L.A. Ganzevles, C.W.M. van der Geld, Marangoni convection in binary drops in air cooled from below, Int. J. Heat Mass Transfer 41 (1998) 1293–1301.
[8] DIN 1952, Durchflussmessung mit Blenden, Düsen und Venturirohren in voll durchströmten Rohren mit Kreisquerschnit, Beuth Verlag GMBH, Berlin, 1982 (in German).
[9] Y. Delclaud, Surface temperature measurements of thin films in the range −100–100 °C using infrared thermograph, in: Proceedings of the Eurotherm Seminar no. 27 (QIRT 92), 1992, pp. 353–358.
[10] F.L.A. Ganzevles, C.W.M. van der Geld, Interfacial and plate temperature histories during dropwise condensation in the presence of noncondensables, in: M. Lehner, D. Mewes (Eds.), Optical Measurements, Springer, Berlin, 1999, pp. 171–184.
[11] A.W.J.P. den Boer, C.W.M. van der Geld, Thermocapillary convection in a liquid layer heated from above, in: G.P. Celata, P. di Marco, A. Mariani (Eds.), 2nd European Thermal Sciences and 14th UIT National Heat Transfer Conference, ETS, Pisa, 1996, pp. 779–786.
[12] F.L.A. Ganzevles, C.W.M. van der Geld, On the prediction of condenser plate temperatures in a cross-flow condenser, in: G.P. Celata, P. di Marco, A. Goulas, A. Mariani (Eds.), Proceedings of the 5th World Conference on Experimental Heat Transfer, Fluid Mechanics and Thermodynamics, Edizioń ETS, Thessaloniki, 2001, pp. 375–380.
[13] S.J. Kline, F.A. McClintock, Describing uncertainties in single-sample experiments, Mech. Eng. 75 (1953) 3–8.
[14] C.W.M. van der Geld, H.J.H. Brouwers, The mean condensate heat resistance of dropwise condensation with flowing, inert gases, Heat Mass Transfer 30 (1995) 435–445.
[15] F. Weitz, C.W.M. van der Geld, F.L.A. Ganzevles, A. Lexmond, The effect of inserts on heat transfer, drainage and gas cleaning efficiency of plastic exchangers, in: R.K. Shah (Ed.), Compact Heat Exchangers and Enhancement Technology for the Process Industries, Begell House, New York, 1999, pp. 507–513.
[16] C.W.M. van der Geld, F.L.A. Ganzevles, C.T.P.F. Simons, F. Weitz, Geometry adaptations to improve the performance of compact, polymer condensers, Trans. IChemE. 79A (2001) 357–362.
[17] F.L.A. Ganzevles, C.W.M. van der Geld, Convective heat transfer in dropwise condensation of multicomponent mixtures with inert gases, 2002, to be submitted.